Plasma Phys. Control. Fusion **52** (2010) 015001 (13pp) doi:10.1088/0741-3335/52/1/015001

Characteristics of energy transport of Li-conditioned and non-Li-conditioned plasmas in the National Spherical Torus Experiment (NSTX)

S Ding[1], S M Kaye[2], R E Bell[2], R Kaita[2], H Kugel[2], B P LeBlanc[2], S Paul[2] and B Wan[1]

[1] Chinese Academy of Sciences Institute of Plasma Physics, PO Box 1126, Hefei, Anhui, 230031, People's Republic of China
[2] Princeton Plasma Physics Laboratory, Princeton University, Princeton, NJ 08543, USA

E-mail: skaye@pppl.gov

Received 2 July 2009, in final form 16 October 2009
Published 24 November 2009
Online at stacks.iop.org/PPCF/52/015001

Abstract
The transport properties of National Spherical Torus Experiment (NSTX) plasmas obtained during the 2008 experimental campaign have been studied and are reported here. Transport trends and dependences have been isolated, and it is found that both electron and ion energy transport coefficients have strong dependences on local values of $n\nabla T$, which in turn is strongly dependent on local current density profile. Without identifying this dependence, it is difficult to identify others, such as the dependence of transport coefficients on B_p (or q), I_p and P_{heat}. In addition, a comparison between discharges with and without lithium wall conditioning has been made. While the trends in the two sets of data are similar, the thermal transport loss, especially in the electron channel, is found to strongly depend on the amount of lithium deposited, decreasing by up to 50% of its no-lithium value.

1. Introduction

The limiter, divertor plates and first wall (FW) in a high performance, and especially burning, tokamak device will experience high particle and heat loads. Work done for the ITER project has indicated that there could be serious problems with the conventional design of a divertor and divertor plates in a steady-state burning plasma fusion device using low Z solid materials as plasma facing component (PFC) materials [1]. Furthermore, some high heat resistant high Z materials such as tungsten may not be suitable for the next-step fusion device because of the possible plasma contamination by these materials. The idea of using liquid metals as a PFC material in fusion devices has been explored as an alternative way of handling these high heat and particle loads [2–6]. The fluid character, as well as the magnetohydrodynamics

(MHD) features of molten salts and liquid metals, especially liquid lithium, has been intensively investigated by the APEX team using simulation and laboratory experiments [7]. Also, related experiments were conducted in some tokamak devices, such as TFTR [8–13], TdV [12], CDX-U [14], FTU [15] and DIII-D [16]. The lithium divertor/wall showed a number of advantages for removing incident tritium and impurity effluxes, providing a self-healing plasma facing surface in a diverted high power DT reactor [7, 17, 18], and enabling a lithium wall fusion regime [19]. Increases in the electron temperature, decreases in recycling and resulting control over the plasma density, suppression of ELMs and a strong reduction in the plasma resistivity were observed in the lithium experiments [20, 21]. Moreover, advanced R&D and experiments showed that a lithium divertor/wall (perhaps with capillary porous system (CPS)) could withstand high heat flux with a shielding layer that could absorb the major part (∼97 to 99%) of the plasma energy [17, 22]. Due to central fueling and low-recycling regimes that could be achieved by using a lithium wall, enhanced stability and energy confinement were suggested as also being possible [19]. For the National Spherical Torus Experiment (NSTX), there has been a long term plan of developing a lithium conditioning capability, starting out with the present capability of lithium evaporation onto the walls, and leading to the installation and operation of a Liquid Lithium Divertor in 2010. Moreover, great success in construction and physics analysis has been achieved [23, 24]. In spite of the virtues expected on lithium wall and the success achieved today, there is still no direct report about the plasma energy transport properties under the influence of lithium in tokamak experiments.

The purpose of this paper is to address the local energy transport properties of the NSTX plasmas both with and without lithium. In the following section, the criterion of choosing experiment data in the database will be explained, as well as the analysis tools and assumptions. After that, the results and discussion will be presented, followed by the conclusions. We find that many of the transport trends in discharges with lithium evaporation are similar to those without, although the lithium conditioned discharges exhibited a reduction in thermal energy transport, especially in the electron channel.

2. Experimental data and transport analysis

The NSTX is a low aspect ratio tokamak with $R_0 \sim 0.85$ m, $a = 0.65$ m ($R/a \sim 1.3$), B_T up to 0.55 T, I_p up to 1.2 MA, κ up to 2.5, δ up to 0.8, and the plasmas, either deuterium or helium are heated with up to 7 MW of D^+ neutral beams with energies up to 100 keV. The discharges used for this study were D^+ into D^0. NSTX is equipped with up–down symmetric, close-fitting, graphite-coated copper conducting walls. Lithium evaporation onto the walls is accomplished by two evaporators, situated in the top divertor area. The lithium is introduced into the vessel by heating the lithium in the main evaporator reservoirs to a temperature of 600 to 650 C. The lithium is directed primarily into the lower divertor region. When used for the experiments to be reported here, the lithium was deposited at a rate up to approximately 15 mg min^{-1} between shots. The lithium evaporation eliminated the need for between-shots helium glow discharge conditioning, which was typically used when lithium was not being used.

The data used for this study were produced in NSTX experiments that were run from April to July 2008. The data chosen for the study to be presented here had to meet several criteria. First, the discharges must have reached a quasi-steady state (e.g. small dW/dt, where W is total plasma energy), with sufficient discharge length (>500 ms). The 'steady-state' period needed to be in excess of 75 ms during the flat top of the plasma current. In practice, a change (increase or decrease) in stored energy up to 10% during this quasi-steady period was allowed. Further, only discharges with no transients in the loop voltage and only low-level

MHD (e.g. low-frequency, AE-modes) were chosen. Discharges with neutral beam heating only were chosen for the study.

The transport analysis of these shots was performed using the TRANSP analysis code [25, 26], which uses the experimental data of NSTX, such as the electron temperature and density from Thomson scattering, the carbon temperature, density and toroidal rotation velocity from charge-exchange recombination spectroscopy, visible bremsstrahlung radiation, plasma current, radiated power profiles and neutral beam information. The plasma equilibrium information is obtained from the magnetic reconstruction EFIT code. The beam deposition subroutine is a full Monte Carlo code, which calculates the sources and losses of these fast particles. For the selected shots, the fast neutral beam ions were assumed to behave classically, and agreement between the measured neutron emission rates and the ones calculated in TRANSP was obtained by adjusting the neutral density boundary condition to values between 10^{10} and 10^{12} cm^{-3}. With this leverage, no anomalous fast ion lost or redistribution of the fast ions due to MHD activity was necessary. For each TRANSP run, a careful examination of electron and ion power balance was carried out to select a time of interest, at least 30 ms after a change in neutral beam power, within the quasi-steady period. This was done to make sure the time rates of change in the electron and ion stored energy were relatively small components in the power balance. These time slices, whose number is 103, constitute the database of transport analysis results used for this analysis. This collection is made up of 43 pre-lithium evaporation, 33 with-lithium conditioning and 27 no-lithium conditioning time slices. The pre-lithium discharges were obtained during the portion of the run where no lithium was yet introduced into the vessel. The no-lithium cases are those after which lithium conditioning had been started, but no lithium was introduced into the vessel just before that particular discharge. As will be seen, various parameters calculated by the transport analysis will be used for this study. The average random uncertainties for the set of variables used (χ_e, χ_i, $n\nabla T_e$, P_{heat}, τ_e) are approximately (10%, 12%, 10%, 12%, 15%), respectively, for most of the locations of interest.

3. Results

3.1. Discharges with no lithium evaporation

In order to understand the influence of lithium on plasma energy transport properties, it is necessary to first study the transport trends in discharge with no lithium, where the range of operating space was broader. The transport trends for discharges with and without lithium were found to be similar when it was possible to compare the two sets over a similar range of parameter variations.

Prior to examining the variation of the energy transport coefficients on the various 'standard' parameters, it is important to identify hidden parameter variations. One such dependence is on the local value of the electron temperature gradient, $-n\nabla T_e$. This dependence is readily seen when examining the relation between local electron diffusivity and poloidal magnetic field B_p at fixed toroidal field B_t, plasma current I_p and heating power P_{heat}. Knowing this dependence is necessary to isolate this trend in figure 1.

The total heating power, as given for the figure and throughout the paper, is defined as $P_{heat} = P_{NBI} + P_{OH} - P_{loss} - dW/dt$, where $P_{loss} = P_{st} + P_{bo} + P_{cx}$, with the individual fast ion loss channels corresponding to shine-through (st), bad orbit (bo) and charge-exchange (cx), respectively. Figure 1 shows the dependence of electron thermal diffusivity on poloidal magnetic field at a radial position of $x = 0.65$, where x is a magnetic flux coordinate defined as the square root of the normalized toroidal flux ($\sqrt{\Phi/\Phi_a}$). The color bar on the right shows the

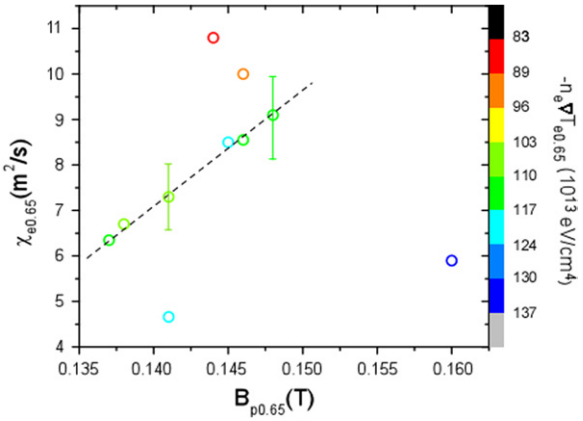

Figure 1. χ_e versus B_p at $x = 0.65$ for the discharges with $I_p = 900\,\text{kA}$, $B_t = 0.48\,\text{T}$ and $P_{heat} = 5.6\,\text{MW}$. The color coding shows values of $-n\nabla T_e$ in units of $10^{13}\,\text{eV cm}^{-4}$. Points along the dashed line have similar $-n\nabla T_e$.

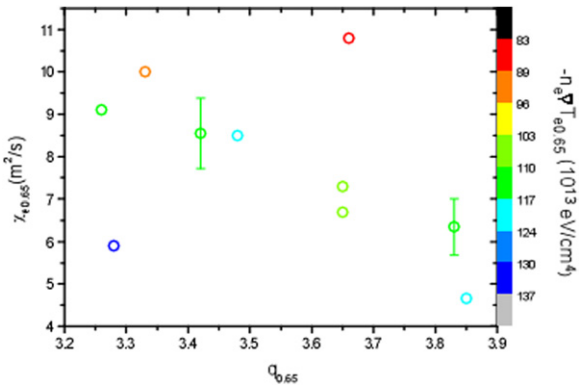

Figure 2. χ_e versus q at $x = 0.65$ for the discharges $I_p = 900\,\text{kA}$, $B_t = 0.48\,\text{T}$ and $P_{heat} = 5.6\,\text{MW}$. The discharges used for this figure were taken from the pre-lithium evaporation run period.

$-n\nabla T_e$ values of data in this figure (B_p in T, n_e in $10^{13}\,\text{cm}^{-3}$, $T_{i,e}$ in eV). If one only focuses on the data points with similar $-n\nabla T_e$ values (in this case the green and light blue points), a proportional relation between χ_e and local B_p can be found. In addition, data points with small $-n\nabla T_e$ values tend to appear in the high-χ_e region, while points with large $-n\nabla T_e$ values are likely to be in the low-χ_e region. Similar trends were found in the plots of both ion and election thermal diffusivities as functions of poloidal field at different radial positions as well as different plasma parameters, both with and without lithium evaporation. Since $B_p \sim B_t/q$, it is not surprising to find out the following result in figure 2, which shows an inverse dependence of χ_e on q over a limited range of $-n\nabla T_e$, at fixed I_p and B_t. This relation is observed in cases both with and without lithium evaporation. In figures 1 and 2, the range in $B_{p0.65}$ and $q_{0.65}$, respectively, at constant B_T, I_p and P_{heat} is due to data being chosen at different times in the different discharges, when the current profiles were still evolving.

The influence of heating power on the thermal diffusivities has also been investigated. To understand this relation, however, it is necessary to understand the dependence of the local

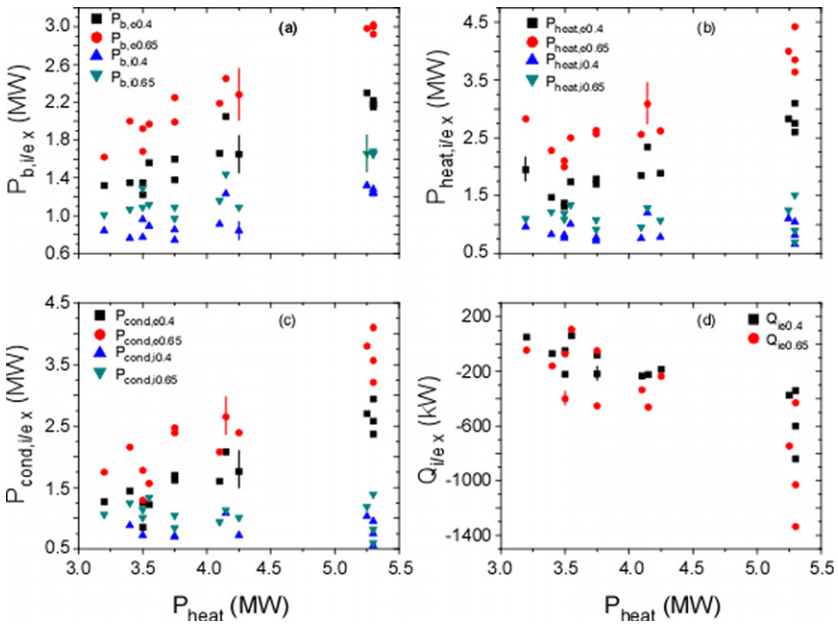

Figure 3. Heating powers volume integrated to $x \sim 0.4$ and 0.65 versus total heating power, P_{heat}, at $I_{\text{p}} = 900$ kA and $B_{\text{t}} = 0.48$ T. (*a*) Beam heating power; (*b*) total heating power; (*c*) conduction loss power; (*d*) ion-election coupling power.

heating powers, conduction loss and ion–electron coupling on the total heating power (as defined above). Figure 3 shows these relations. Shown are the dependences of the (*a*) local beam-collisional heating of ions and electrons, (*b*) local heating power (determined separately for ions and electrons), (*c*) conduction heat loss and (*d*) ion–electron coupling on the total heating power (volume integrated to the boundary, $x = 1.0$) for two different radii, $x = 0.4$ and 0.65. The local beam-collisional heating (*a*) is seen to be strictly proportional to the total heating power, while the local net heating (subtracting loss terms) exhibits an increasing linear relation only for the electrons (*b*). Similarly, while the conduction loss power increases linearly with heating power for the electrons, little change is seen for the ions (*c*). The lack in increase of net ion heating and/or conduction loss with total heating power is due to the increase in the ion–electron coupling, with a net power flow from ions to electrons, with increasing total heating power (*d*). The ion–electron coupling is a more significant component of the ion power balance than for the electrons, as indicated by the size of this term relative to the collisional heating term. Since the incremental electron conduction loss is essentially the same as the incremental net electron heating power, an increase in electron temperature commensurate with the increased total heating power is not seen.

Multiple linear regression analysis of this limited set of discharges indicates no strong statistical relation between the inferred diffusivities and combinations of discharge parameters already discussed (e.g. I_{p}, B_{T}, B_{p}, n_{e} and P_{heat}) either local or global, other than those that define χ. In particular, $\chi_{\text{i/e}}$ at either $x = 0.4$ and 0.65 scales almost linearly with $P_{\text{heat,i/e}}/n_{\text{e}}(-\nabla T_{\text{i/e}})$ locally, which is not surprising considering the convective and radiative losses are minor components of the electron power balance. Not including all or some of these parameters in subsequent analyses led to poor fits, with coefficients of determination <0.3. Here, the coefficient of determination is defined as $R^2 = 1 - \sum_i (y_i - f_i)^2 / \sum_i (y_i - \bar{y})^2$ where y_i are the data points, f_i are the predicted values and $\bar{y}$ is the mean of the data.

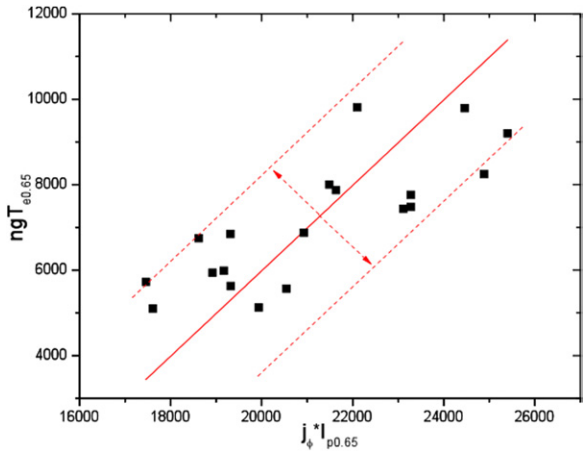

Figure 4. $-n\nabla T_e$ versus $j_\phi I_{px}$ at $x \sim 0.65$, constant $I_p = 900$ kA, $B_t \sim 0.49$ T and $P_{heat} \sim 3.2$–5.3 MW.

3.1.1. Influence of the current profile on $-n\nabla T$ and χ. It was shown that $-n\nabla T$ is important for understanding the dependence of energy transport coefficients on other parameters. Here, it is shown that $-n\nabla T$ can be related directly to the current profile from simple consideration of the plasma equilibrium. If we only consider the force balance equation and take the parameter gradients in the radial direction, we have $\nabla p = \vec{j} \times \vec{B} \rightarrow -n\nabla T + T\nabla n = j_\theta B_\phi - j_\phi B_\theta$. In NSTX, $B_p/B_t \sim B_\theta/B_\phi \sim 0.2$–$0.3$, but $j_\theta/j_\phi \sim \frac{1}{40} \ll 1$. It is, therefore, acceptable to neglect the term containing j_θ. The term, $T\nabla n$, is treated as an intercept. Although this term is not always smaller than $-n\nabla T$, it does not have a significant influence on the trend to be reported (this will be demonstrated later). It is then found that $-n\nabla T \sim j_\phi B_\theta \sim j_\phi (I_{px}/r)$, where j_ϕ is the local plasma current density and I_{px} is the area integral of j_ϕ from zero to the local position, i.e. the plasma current contained inside the local position. At any specific radial position, the relation $-n\nabla T \sim j_\phi B_p \sim j_\phi I_{px}$ applies.

Figure 4 shows a general linear trend between $n_e\nabla T_{e0.65}$ and $j_\phi I_{p0.65}$ (j_ϕ in A cm^{-2}, I_{px} in kA). In this treatment, the local $T\nabla n$ value enters as an intercept. This value varies from shot-to-shot, which, along with other variables such as rotation that enters into the equilibrium, leads to some scatter in the data, as is seen in the figure. Nevertheless, the errors and shot-to-shot variability in these parameters are not great enough to impact the general linear trend seen in the plot.

In order to study the influence of the plasma current on energy transport, the dependence of ion conduction loss power on $-n\nabla T_i$ and local q at constant B_t, P_{heat}, $x = 0.4$ and different I_p is plotted in figure 5 as an example.

As is seen in the figure, there is no obvious dependence of the ion conduction loss on total I_p. It is not the total plasma current itself, which affects P_{cond} directly, but rather $j_\phi I_{px}$. It has been seen that considering $-n\nabla T$ is critical to understanding the relation between χs and B_p. Moreover, $-n\nabla T$ is proportional to $j_\phi I_{px}$, as was seen above. Essentially, this parameter describes the shape or distribution of the plasma current at a specific radial position. While the j_ϕ term represents the local value of the current profile, the I_{px} term the integral value. It was seen in figure 5 that there is a trend for each group of data points that have similar q values toward decreasing $-n\nabla T_i$ as the conduction loss power increases. This indicates that for constant $-n\nabla T_i$, and thus constant $j_\phi I_{px}$, discharges with smaller local q (larger I_{px}, and therefore smaller j_ϕ), will lose more power (larger χ).

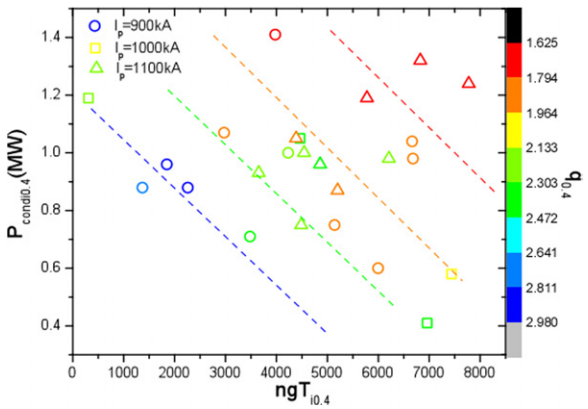

Figure 5. $P_{\rm condi}$ versus $-n\nabla T_{\rm i}$ at $x = 0.4$, $B_{\rm t} = 0.48$ T, $P_{\rm heat} \sim 5$–6.25 MW and multiple total plasma currents.

This trend can also be viewed in the following manner. At constant q, which corresponds to constant $I_{{\rm p}x}$ (dashed lines) larger $-n\nabla T_{\rm i}$ (larger $j_\phi I_{{\rm p}x}$, and therefore larger j_ϕ) corresponds to smaller conduction loss power (smaller χ). Constant $I_{{\rm p}x}$ and large j_ϕ at a specific radial position suggest a flat, even hollow, profile from core region to that position, while larger $I_{{\rm p}x}$ and smaller j_ϕ usually indicates a more peaked profile.

These relations indicate the importance of the plasma current profile to the thermal plasma transport, and this may help also to understand the factors controlling transport in internal transport barrier (ITB) [27] as well as in normal L- and H-mode regimes. Recent work of Bourdelle *et al* [28, 29], provided a possible explanation from the perspective of theoretical analysis. Their work suggested that high $|\beta'| \sim |\nabla p|$ could reduce the drive for the interchange instability due to the ∇B and curvature drifts. Essentially, this is the effect of the so-called α-stabilization in the ballooning formalism. The stabilizing effect of high $|\beta'|$ can induce enhanced temperature and density peaking, leading to even higher values of $|\beta'|$, i.e. a positive feedback loop with respect to turbulence suppression and enhanced confinement. The stabilization of turbulence in this fashion can be partly responsible for ITB sustainment. Although $-n\nabla T$ is mainly discussed in our study, within its validity, i.e. an equilibrium where $\nabla p = \vec{j} \times \vec{B}$ and no significant difference in $T\nabla n$ term, the trend of local ∇p is expected to be similar to that of $-n\nabla T$. The results in this study, therefore, can be considered to be consistent with the explanation put forth in [28, 29], giving some insight into the possible mechanism of the χ dependence on $-n\nabla T$.

3.1.2. The 'pivot' phenomenon in χ profiles. In the previous study on NSTX, Kaye *et al* discovered a kind of 'pivot' phenomenon around $x = 0.5$ in $\chi_{\rm e}$ profiles as a function of $B_{\rm t}$ [30, 31]. The $\chi_{\rm e}$ profile was flat for low $B_{\rm t}$, while it was high in the core and low at the edge for the highest $B_{\rm t}$, pivoting about the $x = 0.5$ position. For an intermediate value of $B_{\rm t}$, the $\chi_{\rm e}$ profile was intermediate between the two extremes. Here, we show that the variation of $B_{\rm t}$ is not the fundamental cause of the 'pivot' phenomena in $\chi_{\rm e}$ profiles. Figures 6(*a*) and (*b*) give examples of the 'pivot' $\chi_{\rm e}$ profiles at constant $I_{\rm p}$, $B_{\rm t}$ and similar $P_{\rm heat}$ taken from the set of discharges used in this study. The total plasma currents are 900 kA and 1100 kA in figures 6(*c*) and (*d*), respectively. The top panels show the $\chi_{\rm e}$ profiles, while the corresponding j_ϕ profiles are given in the bottom panels. The color-coded bands represent the envelope of discharges with similar j_ϕ and $\chi_{\rm e}$ profiles, with the differences in the two bands being due to

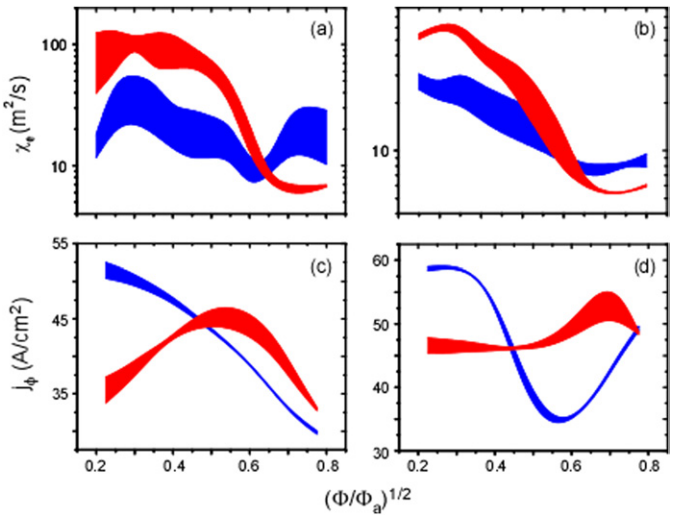

Figure 6. (*a*) χ_e profiles at $I_p = 900\,\text{kA}$, $B_t = 0.48\,\text{T}$ and $P_{heat} \sim 6\,\text{MW}$, (*b*) χ_e profiles at $I_p = 1100\,\text{kA}$, $B_t = 0.48\,\text{T}$ and $P_{heat} \sim 5$–$6\,\text{MW}$, (*c*) plasma current density profiles at $I_p = 900\,\text{kA}$, $B_t = 0.48\,\text{T}$ and $P_{heat} \sim 6\,\text{MW}$, (*d*) plasma current density profiles at $I_p = 1100\,\text{kA}$, $B_t = 0.48\,\text{T}$ and $P_{heat} \sim 5$–$6\,\text{MW}$.

data being taken at different times in the two respective sets of discharges, while the current profile was still evolving. Both sets of profiles were taken from plasmas that did not have lithium conditioning.

This 'pivot' phenomenon can be well explained within the framework of the approach presented in this paper and the above description of the dependences of χ_e on j_ϕ and I_{px}, with low values of χ_e associated with high values of j_ϕ and vice-versa. In fact, it is found statistically that $\chi_{e0.65} \propto j_\phi^{-1.1} I_{px}^{-0.4}$. This fit is shown in figure 7.

Referring back to the experimental data published several years ago [30, 31], it is found that for this data set, j_ϕ varied with B_t at constant I_p. Figure 8 shows an example of this in detail. The solid lines and the dash lines represent χ_e and plasma current profiles, while squares and circles are at low and high B_t, respectively. The results in this figure support the inverse proportional relation between χ and j_ϕ, consistent with the explanation above.

3.2. The influence of lithium on energy transport

The influence of lithium on plasma energy transport will be explored in this section. For discharges with lithium conditioned walls, the lithium was evaporated between shots at various rates. The total thermal energy confinement time, along with the electron energy confinement times at $x = 0.4$ and 0.65 are plotted in figure 9 as a function of the total between-shot deposited lithium prior to the shot of interest. The Li deposition ranges from 0 mg, which are the no lithium baseline discharges for comparison, to over 700 mg for the set of discharges shown in the figure. Increases in the total energy confinement time, as well as the electron confinement times at both radii, are observed. Over the entire range of Li deposition, the total thermal energy confinement time, and especially the electron confinement times, can improve by factors of several. As will be seen, however, there is a rapid increase in impurity accumulation and radiated power losses for Li deposition levels above 400 mg. Below these deposition levels, the confinement improvements are more modest, being only 15% to 20% in

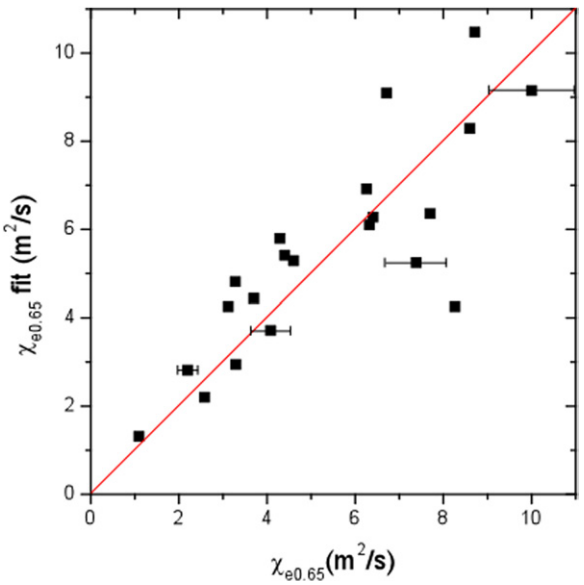

Figure 7. $\chi^{\rm fit}_{\rm e0.65}$ versus $\chi_{\rm e0.65}$ for discharges with lithium evaporation.

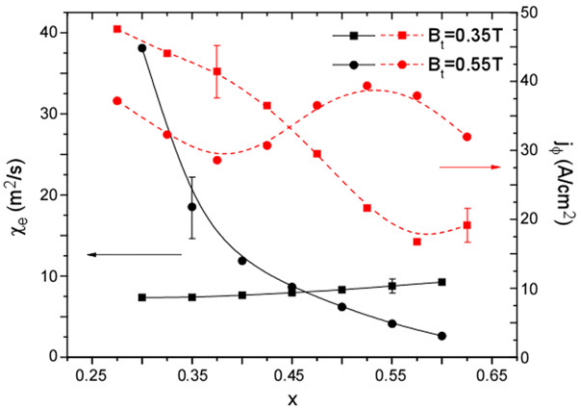

Figure 8. $\chi_{\rm e}$ and plasma current density profiles at $I_{\rm p} = 700$ kA, and $P_{\rm heat} \sim 4$ MW from [30, 31].

the total energy confinement time, but up to 50% to 60% for the electron confinement. This result is consistent with previous results indicating that the improvement in the electron stored energy accounted for the majority of the improvement in the total plasma stored energy [23].

The electron thermal diffusivities are plotted as a function of the total between-shot deposited lithium in figure 10 for two different discharge parameter ranges. The data points at 0 mg lithium are taken from discharges without lithium that had similar plasma parameters to those with lithium. The figures show a nearly linear reduction in the $\chi_{\rm e}$s with increasing Li deposition, up to a factor of 50%, which is consistent with the up to a factor of two increase in electron energy confinement.

It had been reported that enhanced radiated power is associated with increasing lithium deposition [17]. Figure 11 shows the ensemble of $\chi_{\rm e,0.65}$ plotted as a function of lithium

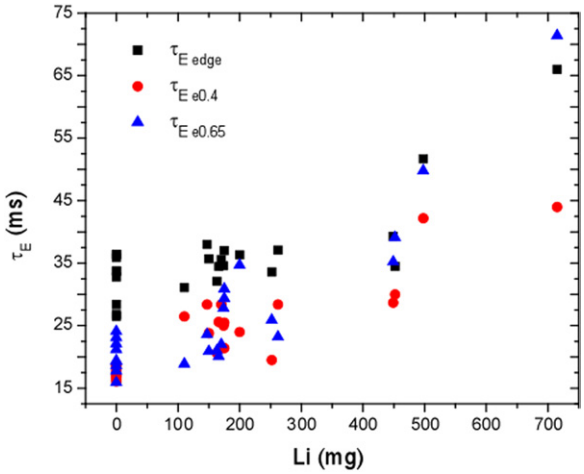

Figure 9. Energy confinement times as functions of the between-shot deposited lithium for each individual discharge at $P_{\text{heat}} \sim 3.8$ MW.

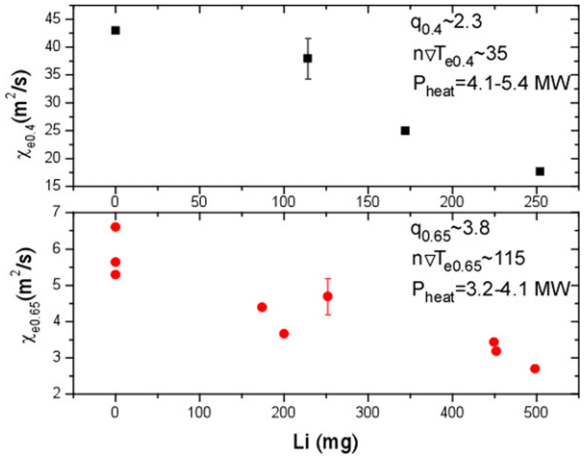

Figure 10. χ_e as a function of the between-shot deposited lithium for each individual discharge at similar local q, $-n\nabla T_e$ and other primary parameter values.

deposition, and color coded by the radiation loss at $x = 0.65$ normalized to the total heating power. The color coding makes it clear that the power radiated is a strong function of the amount of lithium deposited, and this is accompanied by a decrease in the χ_e as discussed above. It was found in NSTX that with sufficient amounts of deposited Lithium ($\geqslant$200 to 300 mg), ELMs were suppressed, leading to an accumulation of metallic impurities in the plasma core and an associated increase in core line radiation. Studies to identify the source of the metallic impurities, and methods to control the accumulation, are underway. The power radiated is seen to exceed 15% of the total heating power for depositions of over 300 mg. With less deposition, up to only 10% of the power is radiated power, but the energy transport in the electron channel can be reduced by 50% or more.

Improvements in the ion thermal diffusivity with increasing lithium deposition are not as clear as they are for the electrons. The histograms shown in figures 12(*a*) and (*b*) attempt to

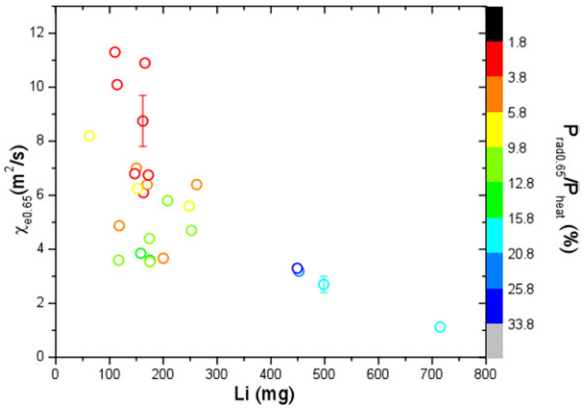

Figure 11. $\chi_{e0.65}$ as a function of the between-shot deposited lithium color coded by (P_{rad}/P_{heat}).

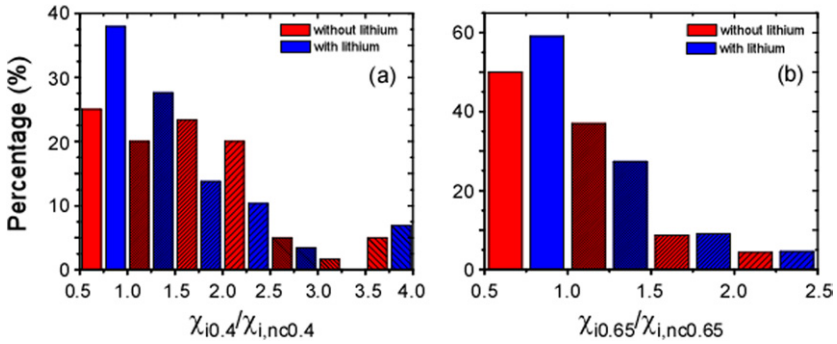

Figure 12. Histogram of $\chi_i/\chi_{i\,nc}$ at (*a*) $x = 0.4$ and (*b*) $x = 0.65$.

illustrate how the ion thermal transport is affected by lithium. The histograms compare the percentage of all discharges, binned by $\chi_i/\chi_{i,nc}$, for discharges with (blue) and without (red) lithium at the two radii $x = 0.4$ (figure 12(*a*)) and 0.65 (figure 12(*b*)). Here, the neoclassical value of the ion thermal diffusivity is obtained using NCLASS [32]. In the figure, each pair of vertical bars (with and without lithium) is actually binned at the same value of $\chi_i/\chi_{i,nc}$. They are separated on the graph only to make the distinction between the two clearer. The histograms indicate that the percentage of low values of $\chi_i/\chi_{i,nc}$ increases for both radii for discharges with lithium. In the absence of direct comparisons of the χ_is between discharges with and without lithium at constant major plasma parameters, these two histograms provide a general indication of the effect of lithium on ion thermal diffusivity.

4. Conclusion

In this study, the local energy transport properties of the NSTX plasmas from the 2008 experimental campaign, both with and without lithium, have been investigated. A significant influence of local $-n\nabla T$ value on the relation between thermal diffusivity and poloidal field was identified, allowing for isolating trends of χ_e with both local B_p and q. Consistent with the above result, it was found that $-n\nabla T \sim j_\phi I_{px}$ at a specific radius, emphasizing the critical role that the plasma current density profile plays in the process of energy transport. This relation

may also be applicable to understanding the reduction in thermal diffusivities in ITBs. This relation also leads to a more fundamental explanation about the 'pivot' phenomena; i.e. the B_t dependence of χ_e as reported in a previous NSTX study. The reduction in electron thermal diffusivity in discharges with lithium wall conditioning was found to be more than 50% of the no-lithium value, and the amount of the reduction depends on the quantity of deposited lithium. The reduction in electron thermal diffusivity with lithium conditioning was more than that expected from the associated increase in power lost due to radiation, indicating a true reduction in thermal losses. Isolating the effect of lithium on the ion thermal transport proved more difficult, but indications were also that χ_i decreased relative to the neoclassical value in discharges that had lithium evaporation.

This study is a further step in understanding the fundamental causes of electron transport in both non-lithium and lithium conditioned discharges. It has brought to light several additional features, such as the role of the current density profile as well as the role that conditioning effects in the outer plasma regions may have on the transport. These effects, such as how lower recycling due to lithium might change the plasma transport and stability characteristics, will be studied in a more systematic fashion in future experiments. The results will provide valuable input for understanding the theoretical underpinnings of electron energy transport.

Acknowledgments

This work was supported by the Chinese National Natural Science Foundation Contract No 10725523, the Chinese Ministry of Science and Technology Contract No 2007DFA01290 and the US Department of Energy Contract No DE-AC02-09CH11466.

References

[1] Frederici G *et al* 2006 *Phys. Scr.* T **124** 1
[2] Kugel H W *et al* 1997 Development of lithium deposition techniques for TFTR *Proc. 17th IEEE/NPSS Symp. on Fusion Engineering (San Diego, CA, 6–10 October 1997)*
[3] Maingi R, Kugel H W and Skinner C H 2000 Physics benefits of liquid metal usage and a review of tokamak experience with lithium *Presented at Workshop on Liquid Metals in NSTX (Princeton, New Jersey, 12 August 2000)*
[4] Kulcinski G L 1979 *J. Nucl. Mater.* **85–86** 87
[5] Moir R W 1997 *Nucl. Fusion* **37** 557
[6] Sokolov Yu A 1995 *Fusion Eng. Des.* **29** 18
[7] Abdou M A *et al* 2004 *Fusion Eng. Des.* **72** 1
[8] Snipes J A *et al* 1992 *J. Nucl. Mater.* **196–1988** 686
[9] Owens D K *et al* 1995 *J. Nucl. Mater.* **220–222** 62
[10] McGuire K M *et al* 1995 *Phys. Plasmas* **2** 2176
[11] Mansfield D K *et al* 1996 *Phys. Plasmas* **3** 1892
[12] Terreault B *et al* 1995 *J. Nucl. Mater.* **220–222** 1130
[13] Sugai H *et al* 1995 *J. Nucl. Mater.* **220–222** 254
[14] Menard J *et al* 1999 *Phys. Plasmas* **6** 2002
[15] Apicella M L *et al* 2008 *35th Conf. on Plasma Physics (Hersonissos, Crete, Greece, June 2008)* vol 32D (ECA) P-4.004
[16] Whyte D G *et al* 2004 *Fusion Eng. Des.* **72** 133
[17] Evtikhin V A *et al* 2002 *Plasma Phys. Control. Fusion* **44** 955
[18] Mirnov S V *et al* 2008 *Proc. 18th Int. Conf. Plasma Surface Interactions (Toledo, Spain, 26–30 May 2008)*
[19] Zakharov L E *et al* 2004 *Fusion Eng. Des.* **72** 149
[20] Majeski R *et al* 2004 *Fusion Eng. Des.* **72** 121
[21] Mansfield D K *et al* 2008 *Proc. 18th Int. Conf. Plasma Surface Interactions (Toledo, Spain, 26–30 May 2008)*
[22] Nygren R E *et al* 2004 *Fusion Eng. Des.* **72** 223
[23] Kugel H W *et al* 2008 *Phys. Plasmas* **15** 056118

[24] Kugel H W *et al* 2007 *J. Nucl. Mater.* **363–365** 791
[25] Hawryluk R J 1979 *Physics of Plasmas Close to Thermonuclear Conditions: (Proc. Course)* vol 1 (Varenna, Italy) p 19
[26] Goldston R J *et al* 1981 *J. Comput. Phys.* **43** 61
[27] Connor J W *et al* 2004 *Nucl. Fusion* **44** R1
[28] Bourdelle C *et al* 2003 *Phys. Plasmas* **10** 2881
[29] Bourdelle C *et al* 2005 *Nucl. Fusion* **45** 110
[30] Kaye S M *et al* 2007 *Nucl. Fusion* **47** 499
[31] Kaye S M *et al* 2007 *Phys. Rev. Lett.* **98** 175002
[32] Houlberg W A *et al* 1997 *Phys. Plasmas* **4** 3230